JOURNAL OF PROPULSION AND POWER
Vol. 23, No. 2, March–April 2007

# Laminar Flame Speeds of Preheated *iso*-Octane/$O_2$/$N_2$ and *n*-Heptane/$O_2$/$N_2$ Mixtures

K. Kumar*
*Case Western Reserve University, Cleveland, Ohio 44106*
J. E. Freeh†
*NASA John H. Glenn Research Center at Lewis Field, Cleveland, Ohio 44135*
and
C. J. Sung‡ and Y. Huang§
*Case Western Reserve University, Cleveland, Ohio 44106*

DOI: 10.2514/1.24391

**Laminar flame speed measurements are carried out for premixed *iso*-octane/air and *n*-heptane/air mixtures under conditions of atmospheric pressure, equivalence ratios ranging from 0.7 to 1.4, and unburned mixture temperatures of 298, 360, 400, and 470 K using the counterflow flame technique. These experiments employ the digital particle image velocimetry technique to characterize the two-dimensional flow field upstream of the flame. As such, the reference stretch-affected flame speed and the imposed stretch rate can be simultaneously determined. By systematically varying the imposed stretch rate, the corresponding laminar flame speed is obtained by linearly extrapolating to zero stretch rate. In addition, the effect of nitrogen dilution level on the laminar flame speed is investigated by varying the nitrogen molar percentage in the oxidizer mixture from 78.5 to 80.5%. These results are further used for the determination of overall activation energies at different equivalence ratios. The experimental laminar flame speeds are subsequently compared with the computed values using two *iso*-octane reaction mechanisms and two *n*-heptane reaction mechanisms available in the literature, followed by discussion and sensitivity analysis.**

## I. Introduction

LIQUID hydrocarbon fuels constitute a bulk of the present day energy sources available for ground and air transportation systems. Practical fuels consist of a wide array of hydrocarbons, including straight chain paraffins such as *n*-heptane, and branched paraffins such as *iso*-octane. Surrogate mixtures of pure hydrocarbons are often used to model the intended physical and chemical characteristics of practical fuels [1]. The choice of constituents in a surrogate mixture is dependent on the aspects of the combustion processes that are targeted for modeling. For practical combustion devices these intended targets include performance criteria such as combustion efficiency, ignition delays, and pollutant formation [2]. *Iso*-octane and *n*-heptane are the primary reference fuels for octane rating and are widely used constituents of gasoline surrogates. *Iso*-octane has also been used as a significant component (5 to 10% by volume) to model surrogate blends for JP-8 [3,4]. These surrogate blends are used both experimentally and computationally to simplify the complex, naturally based mixtures while retaining the fuels' essential properties. In developing surrogate kinetic models, the reaction mechanisms of individual components typically provide the basis for the surrogate model. This implies that the accuracy of the surrogate model is directly dependent on the accuracy of the neat component models.

Laminar flame speed is one of the fundamental properties characterizing the global combustion of a fuel/oxidizer mixture. Therefore, at the global level, laminar flame speed data have been widely used to validate a proposed chemical reaction mechanism. Recognizing that it is important to have experimental data of high fidelity for validating the comprehensiveness of a kinetic mechanism, the present experimental work aims to determine the atmospheric pressure laminar flame speeds of *iso*-octane/air and *n*-heptane/air mixtures over a wide range of equivalence ratios and preheat temperatures. Preheating of air is one of the methods frequently employed in practical combustion devices as a means of waste heat recovery. Fuel preheating is also employed for heavier oils to enable better atomization. Thus, in a majority of practical combustion devices the reactants are in a state of preheat before entering the combustion chamber. There is also interest in the use of liquid hydrocarbon fuels as heat sinks in aeropropulsion devices. This application of liquid hydrocarbon for thermal management could lead to the production of cracked gaseous products from the liquid hydrocarbon under certain conditions and the heating up enhances fuel reactivity [5]. Recognizing the significance of preheating, the effect of mixture preheating on laminar flame speed without fuel cracking is studied and the overall reaction activation energies of varying equivalence ratios are experimentally determined.

In the last decade, the laminar flame speed data for *iso*-octane and *n*-heptane are available from mainly two different experimental techniques, namely the outwardly propagating flame in a combustion bomb and the counterflow or opposed-jet configuration. These two prototypical flames are configurationally simple, and hence facilitate detailed experimentation as well as computational simulation. In addition, for both flame configurations the corresponding methodology of determining laminar flame speed through systematic extrapolation to zero stretch rate is well established. Bradley et al. [6] reported the experimental results on *iso*-octane/air flame speeds using an optically accessible combustion bomb and high speed Schlieren ciné-photography. Their experimental conditions extended over a pressure range of 1 to 10 bar and covered an equivalence ratio range of 0.8 to 1.2 at an initial mixture temperature

Received 2 April 2006; accepted for publication 24 July 2006. 

*Graduate Student, Department of Mechanical and Aerospace Engineering. Member AIAA.
†Aerospace Engineer, Systems Analysis Office, MS 500-103.
‡Associate Professor, Department of Mechanical and Aerospace Engineering; cjs15@case.edu. Senior Member AIAA (corresponding author).
§Research Associate, Department of Mechanical and Aerospace Engineering; currently Combustion Engineer, Ingersoll Rand Energy Systems, Portsmouth, NH 03801. Member AIAA.

of 358 K. They also provided flame speed data at preheat temperatures of 400 and 450 K, for equivalence ratios of 0.8, 1.0, and 1.2. Kwon et al. [7] reported atmospheric flame speed data at a mixture temperature of 298 K and an equivalence ratio range of 0.8 to 1.6 for both *iso*-octane and *n*-heptane fuels by using the outwardly propagating spherical flame configuration. Using the counterflow flame configuration, atmospheric flame speeds of *iso*-octane/air and *n*-heptane/air mixtures have been recently reported by Davis and Law [8] and Huang et al. [9] at 298 K mixture temperature and over a range of equivalence ratios. These stretch-corrected data [6–9] for laminar flame speeds of *iso*-octane/air and *n*-heptane/air flames will be compared with our current work.

Among the aforementioned stretch-corrected flame speed datasets, the work of Bradley et al. [6] is the only known source of *iso*-octane/air laminar flame speeds under conditions of mixture preheating. Using a counterflow facility, this investigation complements the previous endeavors by determining the atmospheric laminar flame speeds of *iso*-octane/air and *n*-heptane/air mixtures over a wider range of preheat temperatures, varying from 298 K to 470 K. In addition, the present study covers equivalence ratios of $\phi = 0.7$ to 1.4 under preheated conditions.

There are several detailed kinetic mechanisms available for *n*-heptane and *iso*-octane. A detailed review of such kinetic models, along with many other hydrocarbons, has been recently discussed by Simmie [10]. Specifically, we will compare the *n*-heptane experimental data with the numerical results obtained using the reaction mechanisms of Davis and Law [8] and Seiser et al. [11]. It is noted that the reaction mechanism of Davis and Law [8] was based on the earlier work of Held et al. [12], with the addition of the *iso*-octane oxidation steps taken from the more detailed model of Curran et al. [13]. The *n*-heptane oxidation mechanism of Seiser et al. [11] was developed based on the extinction and ignition of *n*-heptane in strained laminar flows under nonpremixed conditions. For the comparison of *iso*-octane flame speeds, calculations are conducted using the reaction mechanisms of Davis and Law [8] and Hasse et al. [14]. Furthermore, while the detailed *n*-heptane mechanism of Curran et al. [15] (550 species and 2450 reactions) and the detailed *iso*-octane mechanism of Curran et al. [13] (860 species and 3600 reactions) were validated for both high and low temperature chemistry covering a broad set of equivalence ratios, temperatures, pressures, and $N_2$ dilution ratios, their large size imposes computational constraints and prevents us from making a similar comparison using these two detailed mechanisms.

In the following sections, we shall first detail the experimental setup and the methodology for determining the laminar flame speed. Subsequently, the experimental results will be presented and compared with the computed results using different kinetic mechanisms, followed by sensitivity analysis and discussion.

## II. Experimental Methodology

### A. Burner Setup

The counterflow configuration with two opposed burners is used in the experiments for the determination of laminar flame speed. A schematic of the flow system and the burners is shown inFig. 1.

The nozzle exit diameter is 13 mm and the separation distance between the two nozzles is close to 1 diameter. Both burners are supplied with an identical premixed mixture of vaporized fuel and air. The desired amount of liquid fuel, delivered by a precalibrated syringe pump, is first atomized into fine droplets with the aid of heated nitrogen, and then vaporized in a preheat chamber. The temperature of the preheat chamber is maintained in the range of 373–393 K. Subsequently, the mixture of the fuel vapor and the heated nitrogen is mixed with $O_2$ and/or additional $N_2$ to form a combustible mixture of desired composition. Gas flow rates are regulated using calibrated sonic nozzles. To prevent condensation of fuel vapor, the temperature of the entire flow system containing fuel vapor is maintained at an appropriate temperature by means of heating elements. The temperature control for the various flow subsystems is achieved by means of four temperature controllers. It is ensured that at any location in the flow system the partial pressure of

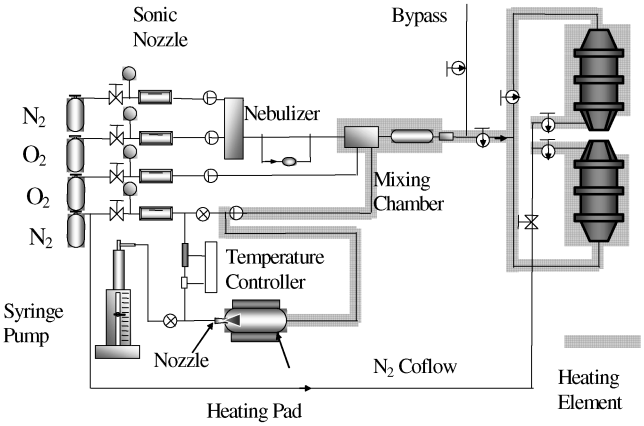


**Fig. 1 Schematic of the current experimental setup.**

fuel vapor in the mixture is well below its saturation value corresponding to the local gas temperature. The resulting unburned mixture temperature is monitored using the thermocouples placed along the nozzle axial centerline at a distance of 4 cm upstream of the nozzle exit for minimal flow interference and yet accurate exit temperature control. A confirmatory check on the mixture temperature is performed manually using thermocouples at each nozzle exit before ignition. Furthermore, because the highest temperatures set in the vaporization chamber and the heated flow system are less than 400 and 500 K, respectively, and the estimated flow residence time in the gas line is less than 2 s, the extent of fuel pyrolysis before fuel being delivered to the burner is expected to be negligible.

A nebulizer is employed to generate seeding particles for the velocity measurement using digital particle image velocimetry (DPIV). Silicone fluid (polydimethylsiloxane) with a viscosity of 50 cS and a density of 970 $kg/m^3$ is used as a seeder. To eliminate the problem of fuel vapor condensation within the nebulizer containing silicone fluid of relatively lower temperature, a part ($\sim$48%) of the oxidizer without any fuel vapors is diverted for seeding particle generation. Subsequently, two separate flow streams comprising of the seeded oxidizer and the unseeded fuel/oxidizer mixture are mixed together in a heated mixing chamber before proceeding to the twin burners. A bypass valve just upstream of the burner is used to vary the flow rate of the combustible mixture through the burners, thereby allowing for the variation of stretch rate while keeping the mixture composition and the seeding density constant. A coflow of heated nitrogen is provided as an inert coannular outer shroud to prevent any interaction with the ambient air and stabilize the flame. For the tests conducted at elevated preheat temperatures, active nozzle cooling is not used. It is observed that the unburned mixture temperature does not change appreciably (no more than 2 K increase) during a typical experimental run time for preheat tests.

### B. Mixture Preparation

The importance of proper premixing and accurate control over the constituent components cannot be overemphasized. In the present experiments, the combustible is a premixed charge of synthesized oxidizer and vaporized fuel. The mixture preparation involves mixing of individual components consisting of nitrogen, oxygen, and the fuel vapor. Controlling the exact mixture composition is one major cause of inaccuracy in the experiments. The situation is further aggravated when a liquid component is introduced. An initial transient in hydrocarbon concentration occurs, dictated purely by the dynamics of the physical systems involved for flows and mixing in an experimental setup. Previous works on the explosion bomb have employed different techniques to ensure that their systems are uniformly mixed, such as using mixing fans [7] or allowing for long duration soaking at elevated temperatures [6].

To verify the composition of the mixture that is fed to the burners in the current experiments, two separate tests are conducted. The first test verifies the composition of the synthesized air and the second

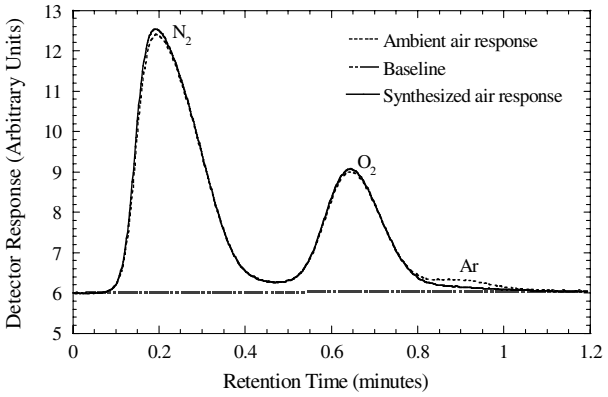


**Fig. 2 Superposed chromatograms of ambient air and synthesized air used in the experiments.**

confirms that there is no loss of fuel due to condensation. These tests also help in determining the time duration required for the flow system to reach steady state in terms of equivalence ratio, and hence ruling out the possibility of any severe liquid flow rate oscillations during experiments. The final uncertainty in the quoted results for the current experiments will be discussed in due course.

The "air" used in the experiments is a mixture of oxygen and nitrogen in the molar ratio of 1:3.76. A gas chromatographic analysis of this synthesized air is carried out and compared with that of ambient air. Figure 2 shows a sample chromatogram obtained for the synthesized air which is superposed on the chromatogram of ambient air under identical test conditions. It is seen that argon is present in the ambient air, but not in the synthesized air. The gas chromatographic results also confirm the composition of the synthesized air employed herein.

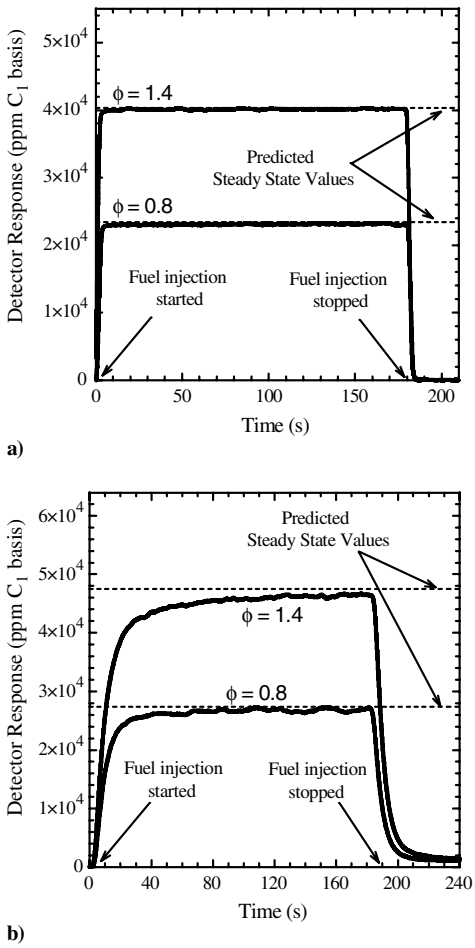


**Fig. 3 Transient response for hydrocarbon buildup in the mixture: a) methane and b) *iso*-octane.**

Further checks are conducted to examine the flow system transient response for hydrocarbon buildup in the mixture to the final desired composition. Samples are collected at the burner inlet and the hydrocarbon detection is conducted by means of a heated flame ionization detector (FID). Both methane and *iso*-octane are used as a representative fuel component for comparison. Methane is used to simulate the addition of gaseous fuel, whereas *iso*-octane represents injection of a liquid fuel into the system. The detector is first zeroed with nitrogen and then spanned with a known concentration of methane in air. Because the premixed charge has a hydrocarbon concentration well in excess of the full-scale range of the FID detector under rich equivalence ratio conditions, sample dilution is employed. The ratio of the amount of air in the diluted sample to the undiluted mixture is 3.5 by volume. The response of the FID, ideally, is linear on a per carbon atom basis. Hence, the response for $C_8$ is expected to be 8 times the methane response for the same molar concentration. In practice, however, a correction factor needs to be applied, which is obtained from the literature [16]. The experimental responses are shown and compared with the predicted steady state values in Fig. 3 for equivalence ratios of 0.8 and 1.4.

It can be seen from Fig. 3 that in the case of a gaseous fuel, steady state is achieved almost instantaneously, whereas for the liquid fuel there can be a transient time of more than 2 min before stable conditions are achieved. The *iso*-octane data also shows that the mean responses for equivalence ratios of 0.8 and 1.4 after reaching steady state, in the time interval of 160–180 s, are, respectively, 97.96 and 97.78% of the predicted values based on the correction factor of [16]. These tests nonetheless demonstrate the adequacy of the present setup for mixture preparation. Figure 3 also illustrates that it will take a longer time for the fuel rich case to reach steady state. Taking note of these response characteristics, the fuel/oxidizer mixture is vented to an exhaust for time durations in excess of its transient time before the flame is ignited for measurements so that experimental repeatability can be assured.

### C. Digital Particle Image Velocimetry Specifications for Velocity Field Measurements

The velocity field of the counterflow configuration is obtained using a planar DPIV system. The mixture flow is seeded using submicron-size particles of silicone fluid, as described earlier. The uniformly dispersed particles in the flow are illuminated by a light sheet of 0.2 mm thickness in the vertical plane using a dual-laser head, pulsed Nd:YAG laser. This laser system generates a 120 mJ/pulse light beam at 532 nm with 3–5 ns pulse width. The light scattered by the seeding particles in the flow field is recorded by a 12-bit, $1280 \times 1024$ pixels Dantec HiSense CCD camera with a pixel pitch of $6.7 \times 6.7$ $\mu$m. The double frame mode of image acquisition is used, and image pairs are acquired at the rate of 4.5 Hz. An optical filter with a passband centered around 532 nm is used to minimize the effects of luminous flame emission on the image. The Dantec particle image velocimetry (PIV) 2100 system is used to control and synchronize the image acquisition and firing of laser pulses, and conduct the subsequent analysis of image pairs using the cross-correlation technique. The field of view is $11.5 \times 9.2$ mm and the magnification $M$ is 0.745. The interrogation subregion size of $32 \times 32$ pixels with 50% overlap being used for cross correlation among the image pairs.

The timing between pulses ($\Delta t$) in these experiments is varied between 50 to 180 $\mu$s. This range of $\Delta t$ is chosen such that for a given equivalence ratio the maximum measurable velocity does not exceed 1.4 times the average reference stretch-affected flame speed over the entire experimental stretch rate range. Because the reference stretch-affected flame speed is used for the subsequent extrapolation to obtain the corresponding laminar flame speed, which will be discussed in Sec. II.F, it is important to keep the accuracy of the measured reference stretch-affected flame speed being close to the full-scale accuracy of the present DPIV setup. In addition, Keane and Adrian [17] have demonstrated that 6 to 10 particles per subregion are required to obtain a high quality PIV correlation. The criteria related to particle number density and particle displacement are

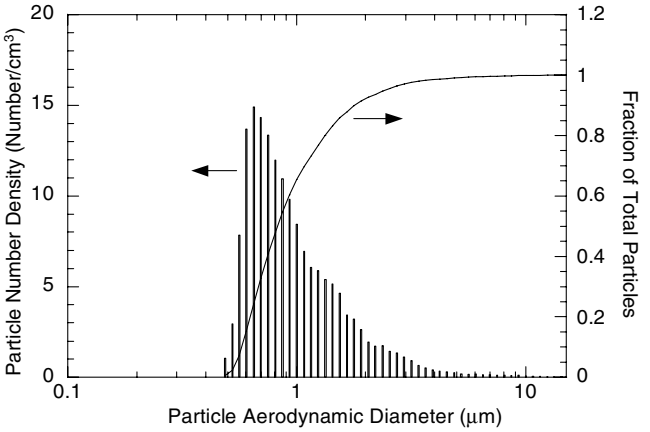


**Fig. 4 Measured particle size distribution for the silicone fluid seeding particles generated.**

ensured to be met in the experiments. The peak-height validation method is applied to validate the instantaneous velocity vector map and remove the spurious vectors. If the ratio of the highest peak to the second highest peak in the correlation plane is less than 1.2, the vector is rejected.

### D. Seeding Particle Size Measurements

A TSI Model 3310A particle sizer is used to experimentally quantify the size distribution of the silicone fluid seeding particles generated by the nebulizer. Several representative flow rates and compositions are analyzed to obtain a complete set of data. A sample plot of the size distribution is shown in Fig. 4, along with the cumulative percentile of the particles counted. It can be seen that $\frac{2}{3}$ of the particles are smaller than 1 $\mu$m in diameter and over 90% are smaller than 2 $\mu$m. These relatively low density, micron-size silicone particles are expected to follow the strained flows studied here [18].

Since the seeding particles do not survive in the post flame zone, it is important to determine how the measured flame speed is affected by the seeding concentration. Using various flame conditions in our earlier work [9], we have compared the raw data with three different particle mass loadings, corresponding to 6, 10, and 17 particles per subregion. Results show that the effect of particle concentration on the measured flame speed is insignificant for the range of mass loading investigated. In the present study, $\sim$10 particles per subregion are used in the measurements.

### E. Measurement Uncertainties

The unburned gas temperature is measured by means of an unsheathed fine gage K-type thermocouple at the nozzle centerline with a wire diameter of 0.25 mm and a bead diameter of 0.52 mm. The maximum uncertainty estimated in the temperature measurement is less than 5 K.

Sonic nozzles for metering gases, such as $N_2$ and $O_2$, are calibrated by a wet test flow meter. The upstream pressure of each sonic nozzle is monitored by a pressure gage with a full-scale accuracy of $\pm 0.25\%$. The uncertainty associated with the mass flow rate of the liquid fuel using the present syringe pump is estimated to be within 1%.

Following [19], the full-scale accuracy in the velocity measurement of the present DPIV is determined by $[(\sigma_t/T)^2 + (\sigma_d/D)^2]^{1/2}$, where $\sigma_t$ is the discriminative minimum period between pulses, $T$ is the period between pulses, $\sigma_d$ the discriminative minimum displacement, and $D$ the maximum displacement determined by the $\frac{1}{4}$ rule. As mentioned earlier, $D$ is 8 for the subregion size of $32 \times 32$ pixels. For particle images spanning 1 to 2 pixels, the discriminative correlation peak position is approximately 0.1 pixels for the three-point Gaussian peak estimators used, namely $\sigma_d$ is 0.1 [20]. The timing error $\sigma_t/T$ is typically negligible using a Nd:YAG laser. For the common Nd:YAG lasers, $\sigma_t \sim 4$ ns. If $T$ is 50 $\mu$s, this yields a small value of the timing error. Consequently, the full-scale accuracy in velocity measurement is equal to $(\sigma_d/D)$, which leads to an accuracy of 1.25% in the present setup.

### F. Determination of Laminar Flame Speed

The vector map obtained by DPIV is further analyzed to determine the reference stretch-affected flame speed and the associated stretch rate. By plotting the axial velocity along the centerline, as shown in Fig. 5a, the minimum axial velocity upstream of the flame location is taken as the reference stretch-affected flame speed $S_{u,\mathrm{ref}}$. Figure 5b further shows that the radial velocity profile at this reference location is linear. Hence, the radial velocity gradient $a$ can be used to unambiguously characterize the flame stretch rate. The stretch rate $K$ is conventionally defined using the axial velocity gradient and is equal to twice the radial velocity gradient, that is $K = 2a$. Based on the variation of $S_{u,\mathrm{ref}}$ with $K$, the unstretched laminar flame speed $S_u^o$ can be determined by the methodology of either linear or nonlinear extrapolation.

Figure 6 plots $S_{u,\mathrm{ref}}$ as a function of Karlovitz numbers $Ka$ for various $n$-heptane/air and *iso*-octane/air flames, with the unburned mixture temperature ($T_u$) of 360 K. The Karlovitz number is defined as $Ka = K\alpha_m/(S_u^o)^2$, where $\alpha_m$ is the thermal diffusivity of the unburned mixture. For each case, the linear extrapolation technique is compared with a nonlinear extrapolation based on the theoretical analysis of Tien and Matalon [21] obtained using a potential flow field. In Fig. 6, the solid and dotted lines represent the linear and nonlinear extrapolations, respectively. It is seen from Fig. 6 that for most of the experimental conditions, $Ka$ is kept to be less than 0.1. Vagelopoulos et al. [22] and Chao et al. [23] have demonstrated that when the Karlovitz numbers are kept to the order of $O(0.1)$, the accuracy of linear extrapolation is improved and the overprediction

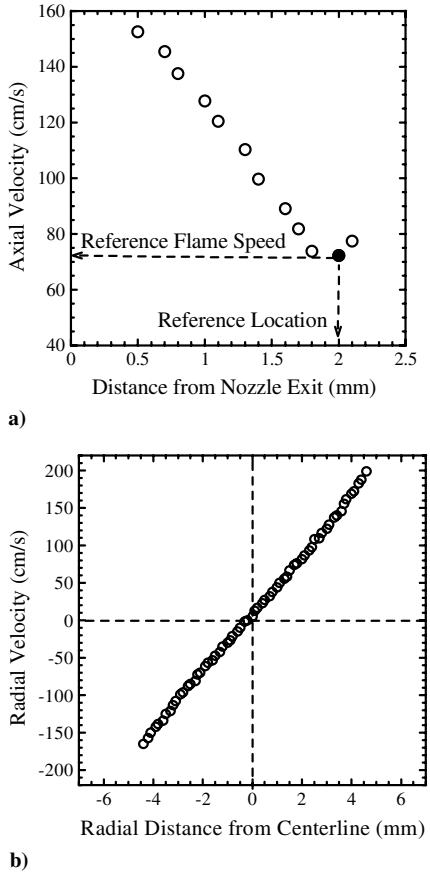


**Fig. 5 a) Centerline axial velocity profile. b) Radial velocity profile at reference location.**

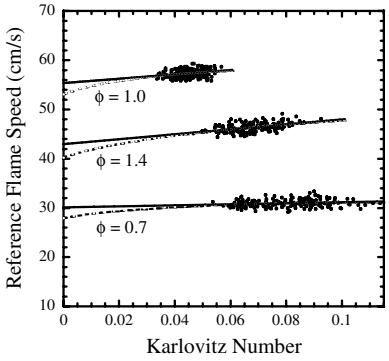


**a) *n*-Heptane/air, $T_u$=360 K**

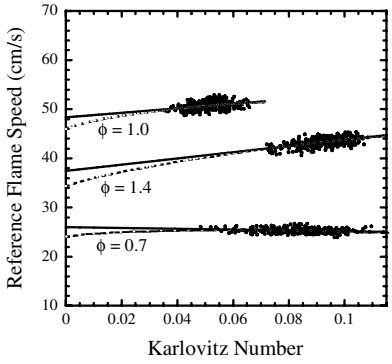


**b) *iso*-Octane/air, $T_u$=360 K**

**Fig. 6 Reference stretch-affected flame speeds as a function of Karlovitz number.**

by linear extrapolation can be reduced to be within the experimental uncertainty. Figure 6 also shows that the linearly extrapolated laminar flame speed is no more than 3 cm/s higher than the value obtained by using a nonlinear extrapolation of Tien and Matalon [21]. Therefore, in the subsequent sections all the laminar flame speeds presented refer to the linearly extrapolated values.

It is also noted that the slope of the $S_{u,\mathrm{ref}} - Ka$ plot reflects the combined effect of stretch rate and nonequidiffusion on flame speed. Figure 6 clearly shows that the flame response with stretch rate variation differs for lean and rich mixtures. Specifically, as $Ka$ is increased, $S_{u,\mathrm{ref}}$ increases for stoichiometric and rich mixtures, but decreases for the mixture of $\phi = 0.7$. This is because the effective Lewis numbers of lean *n*-heptane/air and lean *iso*-octane/air flames are greater than unity, whereas those of rich *n*-heptane/air and rich *iso*-octane/air flames are subunity.

## III. Results and Discussion

### A. Laminar Flame Speeds of *iso*-Octane/Air Mixtures

The laminar flame speeds of *iso*-octane/air mixtures as a function of equivalence ratio for various preheat temperatures are shown in Figs. 7–9. Figures 7 and 8 compare the present experimental data with the literature data for the same or similar $T_u$, whereas Fig. 9 summarizes all the flame speeds of preheated *iso*-octane/air mixtures obtained in the present study. The error bars presented in Fig. 9 indicate the 95% confidence interval estimate of the laminar flame speed obtained by using linear extrapolation [9].

Figure 7 compares the present laminar flame speed data under room temperature condition with those of Davis and Law [8] and Kwon et al. [7]. In general, there is a good agreement between different data sets. In addition, except for $\phi = 1.4$, the present counterflow-based data follow closely with those of Davis and Law [8].

A comparison with the preheated experimental data of Bradley et al. [6] is provided in Fig. 8. It is noted that the work of Bradley et al. [6] defines two burning velocities, one based on the rate of disappearance of cold unburned gas and the second based on the rate

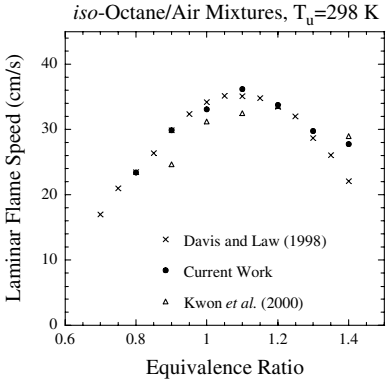


**Fig. 7 Comparison of experimental laminar flame speeds of *iso*-octane/air mixtures for $T_u = 298$ K.**

of appearance of burned gas. Both sets of their data are shown at each equivalence ratio. It is seen from Fig. 8 that the current work is consistent with the available literature data.

The experimental flame speeds are also compared with the computed results using the PREMIX code [24] in conjunction with the CHEMKIN [25] and TRANSPORT [26] packages, originally developed by the Sandia National Laboratories. The computations use windward differencing on the convective term and mixture averaged formulation, and include the thermal diffusion of H and $H_2$. Figures 9a and 9b show the comparisons with the computed flame speeds using the reaction mechanisms of Davis and Law [8] and Hasse et al. [14], respectively. It is seen from Fig. 9 that the mechanism of Davis and Law [8] significantly underpredicts the laminar flame speeds under all conditions of equivalence ratios and unburned mixture temperatures investigated. Such underpredictions worsen as the unburned mixture temperature is increased. On the other hand, the mechanism of Hasse et al. [14] shows a good agreement with the current experimental dataset, especially for the near-stoichiometric conditions at all unburned mixture temperatures investigated. Under lean equivalence ratios, Fig. 9b shows that the

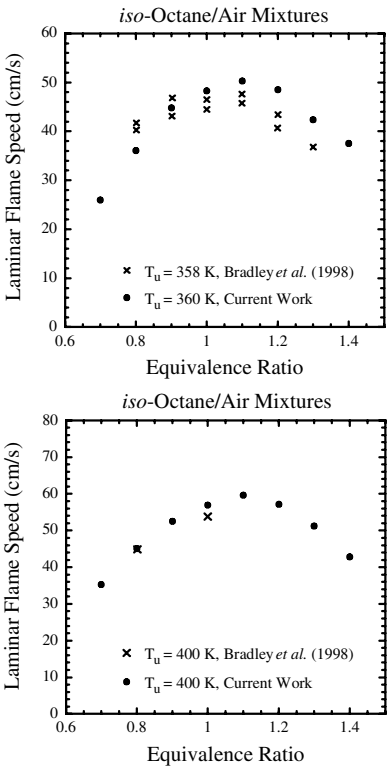


**Fig. 8 Comparison of experimental laminar flame speeds of preheated *iso*-octane/air mixtures.**

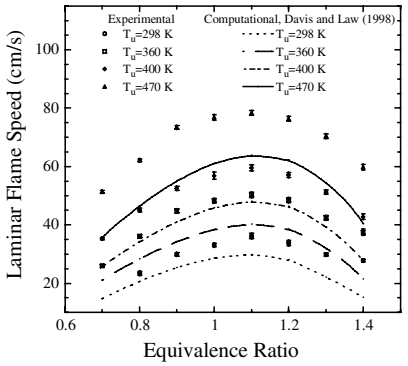


a) *iso*-Octane/Air Mixtures

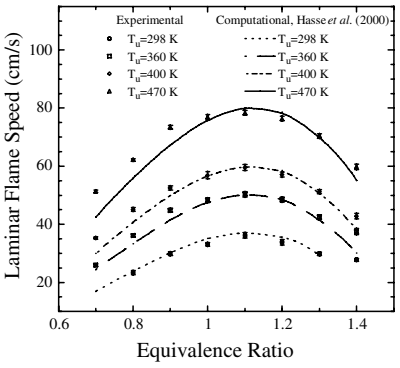


b) *iso*-Octane/Air Mixtures

**Fig. 9 Laminar flame speeds of *iso*-octane/air mixtures for various unburned mixture temperatures.**

mechanism of Hasse et al. [14] underpredict the experimental values. This underprediction is seen to increase as $T_u$ is increased.

### B. Laminar Flame Speeds of *n*-Heptane/Air Mixtures

The laminar flame speeds of *n*-heptane/air mixtures as a function of equivalence ratio are shown in Figs. 10 and 11. Figure 10 compares the present laminar flame speed data under room temperature with those of Davis and Law [8] and Kwon et al. [7]. In contrast to the *iso*-octane/air cases, the comparison of *n*-heptane/air flame speeds among the three datasets is not as good. Specifically, the mismatch is somewhat noticeable for the near-stoichiometric conditions. The measured and computed laminar flame speeds as a function of equivalence ratio for different preheat temperatures are shown in Fig. 11. It is seen that the mechanism of Davis and Law [8] underpredicts the *n*-heptane/air laminar flame speeds by a similar extent as that for the *iso*-octane/air flames. On the other hand, the mechanism of Seiser et al. [11] is found to overpredict the current experimental data except for the conditions of $\phi = 0.7$ and $\phi = 1.4$.

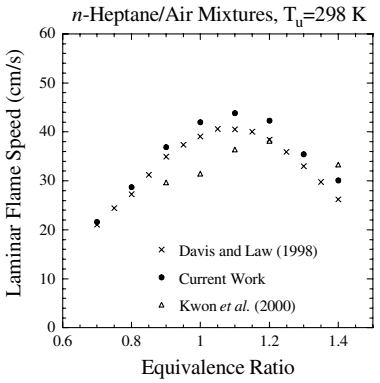


**Fig. 10 Comparison of experimental laminar flame speeds of *n*-heptane/air mixtures for $T_u = 298$ K.**

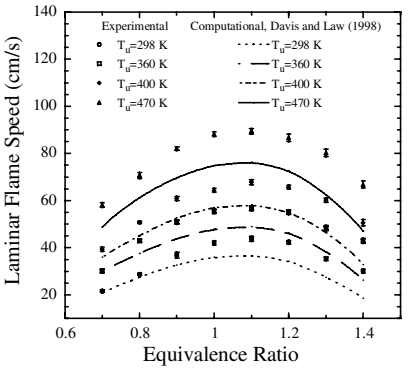


a) *n*-Heptane /Air Mixtures

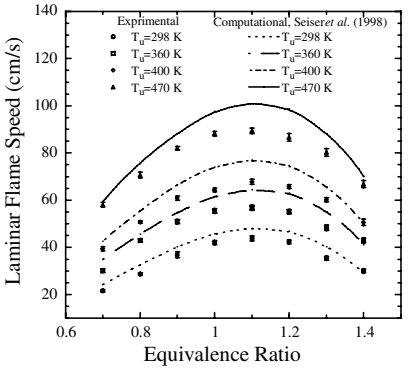


b) *n*-Heptane/Air mixtures

**Fig. 11 Laminar flame speeds of *n*-heptane/air mixtures for various unburned mixture temperatures.**

### C. Comparison of *iso*-Octane/Air and *n*-Heptane/Air Mixtures

Figure 12 summarizes and compares the measured laminar flame speeds of *iso*-octane/air and *n*-heptane/air mixtures obtained in the present investigation. It is seen that the flame speeds of *n*-heptane/air mixtures can be 5–10 cm/s higher than those of *iso*-octane/air mixtures. As discussed in [8,9], because the differences in the flame temperature and transport properties for both fuel/air mixtures are insignificant over the range of equivalence ratios investigated, the difference in laminar flame speed is caused by differences in the chemical kinetics. In particular, the oxidation of *n*-heptane produces a large quantity of ethylene, whereas the main intermediates formed during the *iso*-octane oxidation are propene, *iso*-butene, and methyl radicals [8,9]. As a consequence, the flame speeds of *n*-heptane/air mixtures are higher [8,9].

It is further noted that the mass burning flux $m^o = \rho_u S_u^o$ is a fundamental parameter in the laminar flame propagation, where $\rho_u$ is the unburned mixture density. Figure 13 demonstrates the effect of mixture preheat on the mass burning flux for the fuel lean and stoichiometric cases. Significant enhancement of mass burning flux is observed with increase in the preheat temperature for both *iso*-octane/air and *n*-heptane/air mixtures. Again, for given equivalence ratio and preheat temperature, the mass burning flux of *n*-heptane/air mixture is higher than that of *iso*-octane/air mixture. Figure 13 also shows that in the range of unburned mixture temperatures investigated the mass burning flux increases linearly with $T_u$. As such, the increase in $S_u^o$ with increasing $T_u$ is not only because of the reduction of $\rho_u$.

### D. Effect of Nitrogen Dilution and Determination of Overall Activation Energy

The effect of nitrogen concentration variation on laminar flame speed is also experimentally studied at an unburned mixture temperature of 360 K. Molar percentage of nitrogen in the oxidizer composed of nitrogen and oxygen is varied from 78.5 to 80.5% for three equivalence ratios: $\phi = 0.8$, 1.0, and 1.2. Figure 14 plots the measured flame speeds for both *iso*-octane/oxidizer and *n*-heptane/

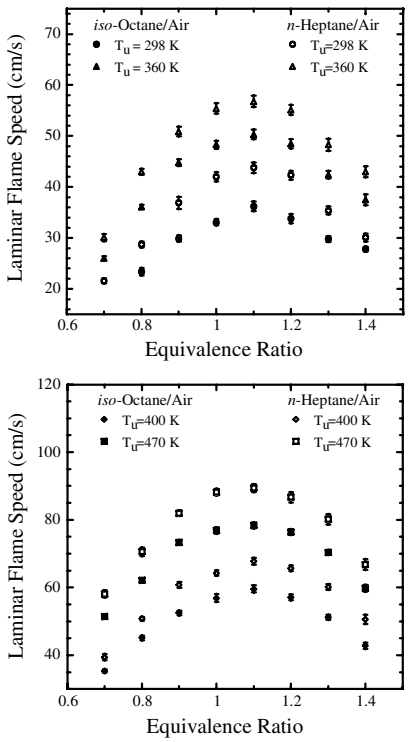


**Fig. 12 Comparison of measured laminar flame speeds for *iso*-octane/air and *n*-heptane/air mixtures.**

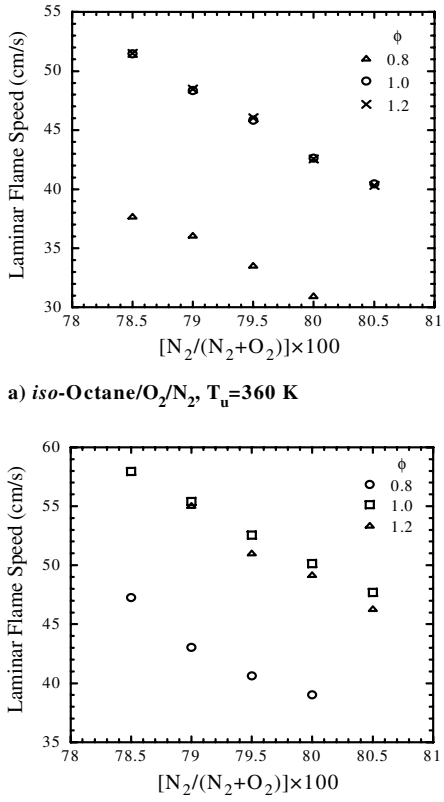


**Fig. 14 Laminar flame speed as a function of molar percentage of $N_2$ in oxidizer $[N_2/(N_2 + O_2)] \times 100$.**

oxidizer mixtures. As expected, the laminar flame speed decreases with increasing level of nitrogen dilution.

Since this range of nitrogen contents, 78.5–80.5%, can be considered as perturbations to that of normal air (79% $N_2$), for a given equivalence ratio the flame speed data at varying nitrogen dilution levels can be employed to deduce the overall activation energy ($E_a$) of the corresponding fuel/air mixture, following the methodology of Egolfopoulos and Law [27]. Namely, the overall activation energy can be determined by

$$E_a = -2R\left[\frac{\partial \ell_n m^o}{\partial(1/T_{\text{ad}})}\right]_p \tag{1}$$

where $T_{\text{ad}}$ is the adiabatic flame temperature and $R$ is the universal gas constant. Because the large scale computational fluid dynamics (CFD) simulations often invoke simplifying kinetics as one-step overall reaction, the extraction of such bulk flame parameter as overall activation energy is especially useful when the CFD calculation with detailed chemistry is not feasible. Based on the experimental results of Fig. 14, the deduced overall activation energies of the three equivalence ratios are shown in Fig. 15a. It is seen that the variation of $E_a$ with $\phi$ is nonmonotonic and peaks near the stoichiometric condition.

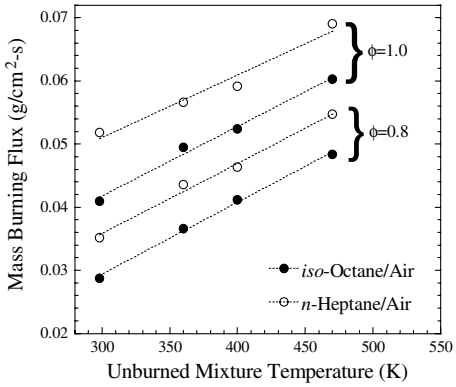


**Fig. 13 Comparison of experimentally determined mass burning fluxes for *iso*-octane/air and *n*-heptane/air mixtures.**

Recognizing that in Eq. (1) $T_{\text{ad}}$ can be perturbed by varying either nitrogen dilution level or preheat temperature, it is of interest to compare the deduced values of $E_a$ using two different methods. Note that the former method perturbs the reactant concentrations by keeping $T_u$ constant, whereas the latter method perturbs the premixed flame system without changing the reactant concentrations. In addition, the linear variation of $m^o$ with $T_u$ demonstrated in Fig. 13 implies the validity of the extraction method through the changes in mixture preheat. Based on the experimentally determined $m^o$ of *iso*-octane/air and *n*-heptane/air mixtures and Eq. (1), Fig. 15b shows the deduced $E_a$ by varying $T_u$.

Comparison of Figs. 15a and 15b demonstrates that despite the quantitative differences in the deduced values, both extraction methods yield a similar trend in the range of equivalence ratios investigated. The overall activation energy is seen to peak close to the stoichiometric condition and decrease on both the lean and rich sides. In addition, the overall activation energy values for *n*-heptane/air mixtures are observed to be lower compared with *iso*-octane/air mixtures for all equivalence ratios under consideration. This similarity of trend and the differences in absolute values using two different extraction methods are also observed in numerical computations with the available detailed reaction mechanisms. Such a quantitative discrepancy possibly arises out of chemical interactions that occur as a consequence of varying $N_2$ concentration and hence the concentrations of fuel and $O_2$. Since the extraction method by varying $T_u$ does not involve a change in reactant composition, the values shown in Fig. 15b are likely to be a better estimate of the overall activation energy.

### E. Sensitivity Analysis on Mass Burning Flux

Sensitivity analysis on mass burning flux is further conducted using the *iso*-octane mechanism of Hasse et al. [14] and the *n*-heptane mechanism of Seiser et al. [11], because these two

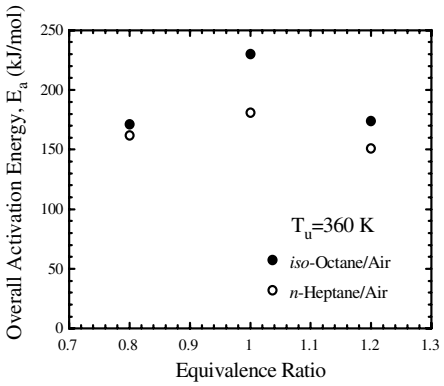


**a) Deduced by varying nitrogen dilution**

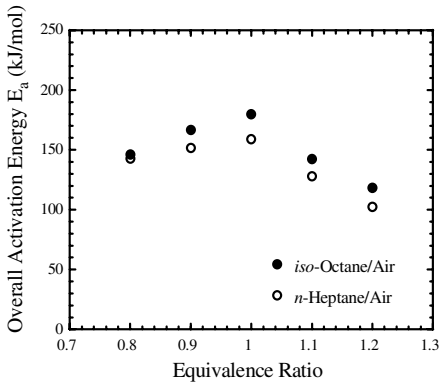


**b) Deduced by varying preheat temperature**

**Fig. 15 Experimentally deduced overall activation energies for *iso*-octane/air and *n*-heptane/air mixtures.**

mechanisms appear to agree better with the present experimental results. Figure 16 plots and compares the normalized sensitivity coefficients of important reactions with respect to the mass burning flux for stoichiometric *iso*-octane/air and *n*-heptane/air flames at two different preheat temperatures. The normalized sensitivity coefficient of the $i$th reaction is defined as $(k_i/m^o)(\partial m^o/\partial k_i)$, where $k_i$ is the reaction rate of the $i$th reaction.

The sensitivity analysis of Fig. 16 shows that the mass burning flux is not sensitive to any of the reactions involving the parent hydrocarbon fuel. As expected, $H + O_2 \rightarrow O + OH$ is the most sensitive reaction enhancing burning rate, and the mass burning flux is also highly sensitive to the CO oxidation reaction, which has a major contribution to the overall heat release. However, the chain initiation reactions involving the breakage of carbon-carbon bonds will always occur and are responsible for the formation of smaller alkenes and hydrogen radicals, which subsequently lead to chain branching reactions [28]. The subsequent hydrogen atom abstraction from the fuel hydrocarbon due to the attacks of radicals leads to the formation of alkyl radicals, which further decompose according to the $\beta$-scission rule into smaller alkenes. Although the products of this decomposition are greatly influenced by the structure of the fuel molecule [28], Fig. 16 indicates the importance of the reactions involving $C_2$–$C_4$ species.

Experimentally obtained profiles for stable species in the work of Bakali et al. [29] for rich atmospheric flames show that the concentrations of unsaturated stable $C_3$ species, namely propene, 1,2-propadiene (allene), and propyne, are significantly higher in the *iso*-octane flames when compared with the *n*-heptane flames, with propyne being the major product. The same work also shows that the major stable $C_2$ specie is ethylene, whereas the relative amount of ethylene is much larger for *n*-heptane flames [29]. It can thus be concluded that the high temperature oxidation kinetics of these unsaturated $C_2$–$C_3$ hydrocarbons along with their significantly different concentrations in the two flames account for the differences in the measured laminar flame speed values. Furthermore, the discrepancies in the prediction of laminar flame speeds using different reaction mechanisms require a better understanding of the $C_2$–$C_3$ chemistry, as has already been pointed out by the previous work of Davis and Law [8].

## IV. Conclusions

Atmospheric laminar flame speeds of *iso*-octane/air and *n*-heptane/air mixtures are experimentally determined over a range of equivalence ratios and unburned mixture temperatures. The present measured laminar flame speeds complement the existing literature data on primary reference fuels and provide a benchmark database for validating the detailed reaction mechanisms at the global level. Under the same equivalence ratio, the flame speed of *iso*-octane/air mixture can be 5–10 cm/s lower than that of *n*-heptane/air mixture depending on the preheat level. The predicted flame speed data for *iso*-octane/air flames using the mechanism of Hasse et al. [14] show good agreement with the measured values. However, the computed flame speeds for *n*-heptane/air mixtures using the reaction mechanisms available in the literature do not agree favorably with our experimental results. The effect of nitrogen dilution on laminar flame speed is also experimentally investigated. In addition, the overall activation energies at varying equivalence ratios are extracted from the experimental data because their relevance to the CFD simulations using one-step reaction. As with the previous findings, the importance of $C_2$–$C_3$ chemistry in the flame propagation of *iso*-octane/air and *n*-heptane/air mixtures is identified and emphasized through sensitivity analysis.

## Acknowledgements

This material is based upon work supported by the National Science Foundation under Grant No. 0133161. The authors would also like to thank Mark Wernet of NASA Glenn Research Center for assistance with the seeding particle size measurements and DPIV analysis.

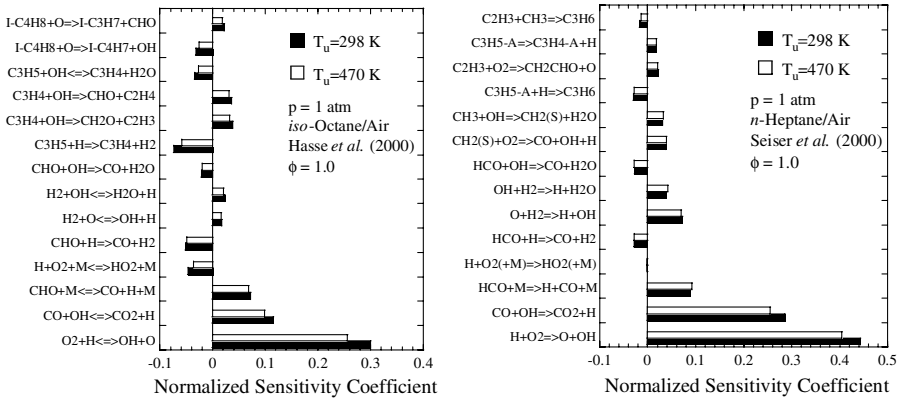


**Fig. 16 Sensitivity analysis using the mechanisms of [11] and [14].**

## References


[1] Violi, A., Yan, S., Eddings, E. G., Sarofim, A. F., Granata, S., Faravelli, T., and Ranzi, E., "Experimental Formulation and Kinetic Model for JP-8 Surrogate Mixtures," *Combustion Science and Technology*, Vol. 174, Nos. 11–12, 2002, pp. 399–417.

[2] Montgomery, C. J., Cannon, S. M., Mawid, M. A., and Sekar, B., "Reduced Chemical Kinetic Mechanisms for JP-8 Combustion," AIAA Paper 2002-0336, Jan. 2002.

[3] Mawid, M. A., Park, T. W., Sekar, B., and Arana, C., "Importance of Surrogate JP-8/Jet-A Fuel Composition in Detailed Chemical Kinetics Development," AIAA Paper 2004-4207, July 2004.

[4] Cooke, J. A., Bellucci, T. W., Smooke, M. D., Gomez, A., Violi, A., Faravelli, T., and Ranzi, E., "Computational and Experimental Study of JP-8: A Surrogate, and Its Components in Counterflow Diffusion Flames," *Proceedings of the Combustion Institute*, Vol. 30, 2005, pp. 439–446.

[5] Curran, E. T., and Murthy, S. N. B. (eds.), *Scramjet Propulsion, Progress in Astronautics and Aeronautics*, AIAA, Reston, VA, 2001, Vol. 189, Chap. 12.

[6] Bradley, D., Hicks, R. A., Lawes, M., Sheppard, C. G. W., and Woolley, R., "The Measurement of Laminar Burning Velocities and Markstein Numbers for *iso*-Octane-Air and *iso*-Octane-*n*-Heptane-Air Mixtures at Elevated Temperatures and Pressures in an Explosion Bomb," *Combustion and Flame*, Vol. 115, Nos. 1–2, 1998, pp. 126–144.

[7] Kwon, O. C., Hassan, M. I., and Faeth, G. M., "Flame/Stretch Interactions of Premixed Fuel–Vapor/$O_2$/$N_2$ Flames," *Journal of Propulsion and Power*, Vol. 16, No. 3, 2000, pp. 513–522.

[8] Davis, S. G., and Law, C. K., "Laminar Flame Speeds and Oxidation Kinetics of *iso*-Octane-Air and *n*-Heptane-Air Flames," *Proceedings of the Combustion Institute*, Vol. 27, 1998, pp. 521–527.

[9] Huang, Y., Sung, C. J., and Eng, J. A., "Laminar Flame Speeds of Primary Reference Fuels and Reformer Gas Mixtures," *Combustion and Flame*, Vol. 139, No. 3, 2004, pp. 239–251.

[10] Simmie, J. M., "Detailed Chemical Kinetic Models for the Combustion of Hydrocarbon Fuels," *Progress in Energy and Combustion Science*, Vol. 29, No. 6, 2003, pp. 599–634.

[11] Seiser, H., Pitsch, H., Seshadri, K., Pitz, W. J., and Curran, H. J., "Extinction and Autoignition of *n*-Heptane in Counterflow Configuration," *Proceedings of the Combustion Institute*, Vol. 28, 2000, pp. 2029–2037.

[12] Held, T. J., Marchese, A. J., and Dryer, F. L., "A Semi-Empirical Reaction Mechanism for *n*-Heptane Oxidation and Pyrolysis," *Combustion Science and Technology*, Vol. 123, Nos. 1–6, 1997, pp. 107–146.

[13] Curran, H. J., Gaffuri, P., Pitz, W. J., and Westbrook, C. K., "A Comprehensive Modeling Study of *iso*-Octane Oxidation," *Combustion and Flame*, Vol. 129, No. 3, 2002, pp. 253–280.

[14] Hasse, C., Bollig, M., and Peters, N., and Dwyer, H. A., "Quenching of Laminar *iso*-Octane Flames at Cold Walls," *Combustion and Flame*, Vol. 122, Nos. 1–2, 2000, pp. 117–129.

[15] Curran, H. J., Gaffuri, P., Pitz, W. J., and Westbrook, C. K., "A Comprehensive Modeling Study of *n*-Heptane Oxidation," *Combustion and Flame*, Vol. 114, Nos. 1–2, 1998, pp. 149–177.

[16] California Air Resources Board, "Procedure for the Detailed Hydrocarbon Analysis of Gasolines by Single Column High Efficiency (Capillary) Column Gas Chromatography," SOP No. MLD 118, Rev No. 1.1, 1997.

[17] Keane, R. D., and Adrian, R. J., "Theory of Cross-Correlation Analysis of PIV Images," *Applied Scientific Research*, Vol. 49, No. 3, 1992, pp. 191–215.

[18] Melling, A., "Tracer Particles and Seeding for Particle Image Velocimetry," *Measurement Science and Technology*, Vol. 8, No. 12, 1997, pp. 1406–1416.

[19] Wernet, M. P., "A Flow Field Investigation in the Diffuser of a High-Speed Centrifugal Compressor using Digital Particle Imaging Velocimetry," *Measurement Science and Technology*, Vol. 11, No. 7, 2000, pp. 1007–1022.

[20] Westerweel, J., "Fundamentals of Digital Particle Image Velocimetry," *Measurement Science and Technology*, Vol. 8, No. 12, 1997, pp. 1379–1392.

[21] Tien, J. H., and Matalon, M., "On the Burning Velocity of Stretched Flames," *Combustion and Flame*, Vol. 84, Nos. 3–4, 1991, pp. 238–248.

[22] Vagelopoulos, C. M., Egolfopoulos, F. N., and Law, C. K., "Further Considerations on the Determination of Laminar Flame Speeds with the Counterflow Twin Flame Technique," *Proceedings of the Combustion Institute*, Vol. 25, 1994, pp. 1341–1347.

[23] Chao, B. H., Egolfopoulos, F. N., and Law, C. K., "Structure and Propagation of Premixed Flame in Nozzle-Generated Counterflow," *Combustion and Flame*, Vol. 109, No. 4, 1997, pp. 620–638.

[24] Kee, R. J., Grcar, J. F., Smooke, M. D., and Miller, J. A., "A FORTRAN Program for Modeling Steady Laminar One-Dimensional Premixed Flames," Sandia National Laboratories, Livermore, Rept. No. SAND85-8240, Dec. 1985.

[25] Kee, R. J., Rupley, F. M., and Miller, J. A., "Chemkin-II: A FORTRAN Chemical Kinetics Package for the Analysis of Gas-Phase Chemical Kinetics," Sandia National Laboratories, Livermore, Rept. No. SAND 89-8009, Sep. 1989.

[26] Kee, R. J., Dixon-Lewis, G., Warnatz, J., Coltrin, M. E., and Miller, J. A., "A Fortran Computer Code Package for the Evaluation of Gas-Phase, Multicomponent Transport Properties," Sandia National Laboratories, Livermore, Rept. No. SAND86-8246B, Mar. 1998.

[27] Egolfopoulos, F. N., and Law, C. K., "Chain Mechanisms in the Overall Reaction Orders in Laminar Flame Propagation," *Combustion and Flame*, Vol. 80, No. 1, 1990, pp. 7–16.

[28] Glassman, I., *Combustion*, 2nd ed., Academic Press Inc., New York, 1987, Chap. 3.

[29] Bakali, A. E., Delfau, J.-L., and Vovelle, C., "Experimental Study of of 1 Atmosphere, Rich, Premixed *n*-Heptane and *iso*-Octane Flames," *Combustion Science and Technology*, Vol. 140, Nos. 1–6, 1998, pp. 69–91.


C. Avedisian
*Associate Editor*